Hole emission processes in InAs/GaAs self-assembled quantum dots

W. -H. Chang, W. Y. Chen, and T. M. Hsu*
Department of Physics, National Central University, Chung-li, 32054 Taiwan, Republic of China

N. -T. Yeh and J. -I. Chyi
Department of Electrical Engineering, National Central University, Chung-li, 32054 Taiwan, Republic of China
(Received 16 July 2002; published 27 November 2002)

We present a study of the hole emission processes in InAs/GaAs quantum dots using capacitance and admittance spectroscopies. From the conductance mapping, the hole levels show a quasicontinuous distribution, instead of the clear shell structures that have been observed in electron systems. According to a comparative analysis of the capacitance and admittance spectroscopies, the hole emission process is identified to be via thermally activated tunneling through the wetting layer as an intermediate state. An energy level diagram of the quantum dot is also constructed, which shows the hole in our quantum dots to be more weakly confined. We propose a general thermally activated tunneling model to explain our results and those in other works. The conclusion is that both the localization energy and the electric field are important for the carrier emission processes. This model is further extended to predict which carrier type (i.e., electron or hole) will be more relevant during the exciton dissociation processes in quantum dots.

DOI: 10.1103/PhysRevB.66.195337 PACS number(s): 73.63.Kv, 73.23.−b, 73.21.La

I. INTRODUCTION

Self-assembled InAs/GaAs quantum dots (QD's) have attracted considerable attention in recent years due to their applications in QD lasers,[1] infrared photodetectors,[2,3] and their potentials in the development of quantum nanodevices.[4] Motivated in part by these applications, a considerable number of studies on InAs/GaAs QD's have been reported.[5] For these devices to operate at room temperature, the thermionic emission of carriers from the QD's is always the main consideration.

The most important inherent factor determining the carrier emission process is the localization energy, i.e., the confinement depth of the electron or hole energy levels in the QD's with respect to the GaAs band edge. Several experiments have been devoted to the investigation of the electron and hole levels separately, either by using electrical[6–11] or optical[11–13] techniques. However, for InAs/GaAs QD systems, a large variety in electron/hole localization energies have been found in different works, ranging from relatively less confined hole levels[13] to relatively more localized hole levels.[9] For example, the capacitance-voltage measurements combined with self-consistent simulation reported by Brounkov *et al.*[9] suggest the holes to be more deeply confined in InAs/GaAs QD's. However, recent midinfrared photocurrent spectroscopy results reported by Chu *et al.*[13] show the localization energy of the electrons to be by far larger than that of the hole.

On the theoretical side, the multiband $\mathbf{k}\cdot\mathbf{p}$ model[14] and empirical pseudopotential theory[15] developments had enabled us to get a deeper insight into the electronic structure of strained InAs/GaAs QD's. However, these model calculations rely strongly on the detailed structural properties of the QD's. Indeed, in the limited number of theoretical works, the calculated localization energies depend not only on the QD's size, shape (whether pyramidal with different facet angles or lens shape with different aspect ratios), inside composition distribution (possibly caused by the interdiffusion or indium aggregations), but also on the input material parameters.[14] For example, the theoretical calculations reported by Stier *et al.*[14] have shown that the relative strength of the electron and hole localization energies were inverted when different values of the InAs/GaAs band offset were chosen. Recent empirical pseudopotential calculations[16] have indicated that the electrons are more localized than the holes for a lens-shaped QD of pure InAs, while the holes become even more confined when a nonuniform In/Ga distribution is introduced.

The mechanisms for electron and hole emissions from InAs/GaAs QD's have also been investigated, most commonly by using the so-called space-charge techniques, such as admittance[10,11,17] and deep-level transient spectroscopies[7,8,18,19] (DLTS), which have long been used to characterize the deep levels[20] and the band offset of various kinds of heterostructures.[21–23] However, the escape mechanisms reported in different works were varied, even when the same experimental techniques were employed.[8,18,19]

Due to the above-mentioned discrepancies, the carrier emission mechanism for the InAs/GaAs QD system needs to be carefully reexamined. This paper is therefore aimed at constructing a more general picture for realizing the carrier emission processes. In this work, we focus on the hole levels and their escape mechanisms by using the capacitance and admittance spectroscopies. The investigation is then completed by a comparison with our previous works on the electron system in similar QD's.[11] We find that, in our InAs QD system, the hole localization is weaker than the electron localization. The hole emission process is found to be a thermally activated tunneling process, via the wetting layer as an intermediate state, instead of the available excited states as observed in electron systems.[7,11] We generalize the thermally activated tunneling model to explain our results and those in other works, concluding that both the localization energy and the electric field are important for the carrier emission pro-

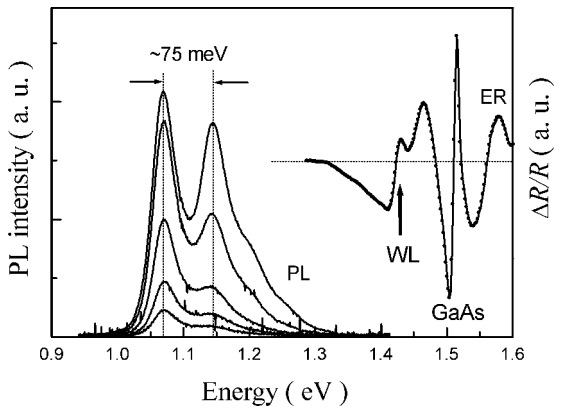

FIG. 1. The PL spectra for the InAs/GaAs QD's taken at $T=10$ K under various excitation conditions. The ER spectrum taken at the same temperature is also displayed.

cesses. Finally, we further extend this model to explain which carrier types will be more relevant during exciton dissociation from the QD's.

II. EXPERIMENTS

To study the hole levels, we incorporated an InAs QD layer into a GaAs n^+-p diode. The sample was grown on an (001)-oriented n^+-type GaAs substrate by solid-source molecular beam epitaxy. An InAs QD layer, sandwiched between two 10-nm nominally undoped GaAs spacers, was embedded in the p-type GaAs region of the n^+-p diode, at a distance of 300 nm above the n^+-p interface. The p-type doping concentration was about $(6\pm1)\times10^{16}$ cm^{-3}. The InAs QD's were formed by depositing 2.7 monolayers of (ML) InAs at 520 °C using the Stranski-Krastanow growth mode, while the growth of the other GaAs layers was maintained at 580 °C under As-stabilized conditions. According to transmission electron microscopy (TEM) studies, the QD's had an average diameter of $18(\pm2)$ nm, were ≈3.5 (±0.5) nm high, and had a sheet density of 3×10^{10} cm^{-2}.

After growth, the sample was processed into square mesas for electrical characterizations. The front electrode was formed by evaporating a metal contact on the mesa top, while the back contact was formed by alloying indium to the n^+-type GaAs substrate. The capacitance-voltage (C-V), conductance-voltage (G-V) and admittance spectroscopies were measured by an HP 4284A LCR meter (20 Hz–1 MHz) operated at a test signal of 20 mV. Temperature-dependent measurements were performed in a close-cycle helium cryostat equipped with a temperature controller having a temperature stability better than 0.5 K.

The sample was first characterized by low-temperature ($T=10$ K) photoluminescence (PL) spectroscopy under various excitation powers, which are shown in Fig. 1. In the PL spectra, two main luminescence peaks, at 1.069 eV and 1.144 eV, can be seen, which are the transitions of the ground states and the first excited states of InAs QD's. The wetting-layer (WL) transition was not observed under the excitation conditions used here. To reveal the WL transitions, electroreflectance (ER) spectroscopy have been performed, which is also included in this figure. The WL signal can be observed in the ER spectrum at ~1.42 eV. This energy approximately corresponds to a ~1.6-ML thick quantum well of pure InAs.[24–26] The estimated WL thickness is also very close to the observed critical thickness (~1.7 ML) during QD formations.

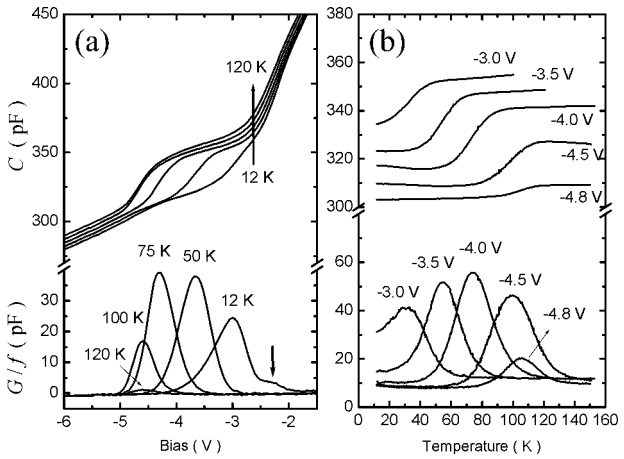

FIG. 2. (a) The temperature evolution of the 500-kHz C-V and G-V spectra measured at $T=12$, 50, 75, and 100 K. Each C-V trace has been offset by 2 pF for clarity. (b) The temperature scans of the admittance spectra measured at different biases.

Figure 2(a) shows the temperature evolution of the C-V and G-V characteristics measured at a test frequency of $f=500$ kHz. Due to the p-type modulation doping in the GaAs matrix, the InAs dots are charged by holes at a zero bias. When a reversed bias is applied to the n^+-p diode, these accumulated holes will be gradually swept out of the dots. For $T>100$ K, a capacitance plateau in the bias range of -2.8 V$\leqslant U\leqslant-4.5$ V can be seen, corresponding to the discharging of the holes in the QD layer.[9,11,27,28] When the temperature is gradually lowered to $T=12$ K, the capacitance plateau is suppressed, accompanied by a conductance peak near the edge of the capacitance plateau. This phenomenon is a manifestation of a nonequilibrium charging/discharging effect.[10,11] In the bias range of -2.8 V$\leqslant U\leqslant-4.5$ V, the Fermi level E_f crosses through the hole levels of the dots. The small ac voltage with an angular frequency $\omega(=2\pi f)$ will alternatively fill and empty the QD hole levels in this bias range. When the characteristic time (τ) for such hole exchanges between the dots and the barrier matched the applied ac frequency ω, i.e., $\omega\tau=1$, a resonant condition is achieved and a conductance maximum ($G_{\max}$) is exhibited. Since the time constant τ depends on both the hole localization energies and the temperature, the applied ac frequency will resonate with different hole levels as the bias and the temperature are varied.

In Fig. 2(b), the admittance spectra for both the capacitance and the conductance measured at different bias voltages are displayed. Since $G_{\max}$ is proportional to the number of holes being exchanged between the dots and the barrier, the experiment of a temperature-bias mapping for the QD conductance can be an alternative way to probe the hole-level distribution in the dots. Figure 3(a) displays a contour plot of such conductance mapping. For comparison purposes,

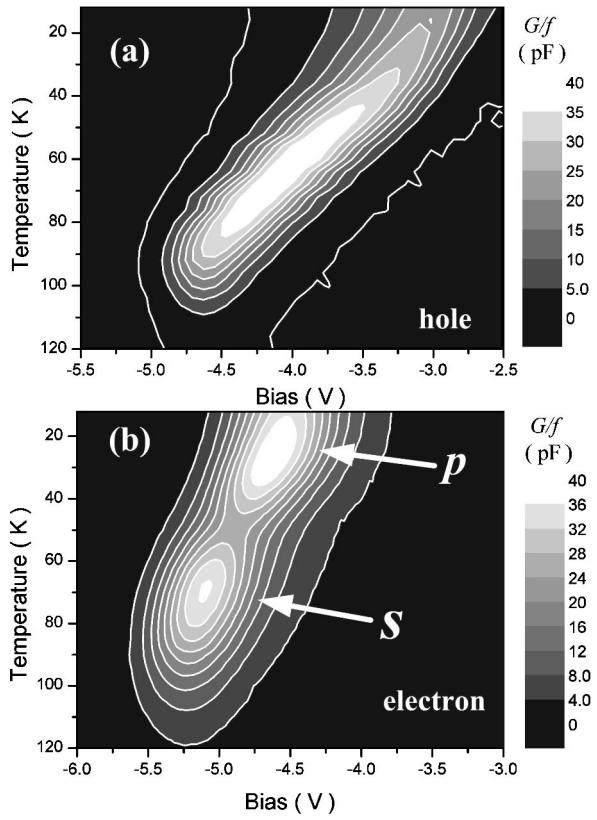

FIG. 3. (a) Conductance mapping of the hole levels in InAs/GaAs QD's. (b) The same conductance mapping for the electron levels in a similar *n*-type sample, as reported in Ref. 11.

we also display in Fig. 3(b) the conductance mapping of electron levels in similar InAs QD's for another *n*-type sample. The capacitance and admittance spectroscopies of this sample have been previously studied (see Ref. 11), where detailed sample structures and experimental results can also be found. In the electron-level spectrum in Fig. 3(b), well-defined shell structures can be seen. However, in contrast, the hole-level spectra presented in Fig. 3(a) display a quasicontinuous distribution. This indicates that the hole-level splitting is quite small, and its discrete nature is smeared out by the inhomogeneous size distribution.

To extract the activation energies of these hole levels, the bias-dependent admittance spectra are analyzed by the following relation,

$$\omega = \omega_0 \exp(-E_A/k_B T_{\max}), \tag{2.1}$$

where ω_0 is a preexponential factor, $T_{\max}$ is the temperature at $G_{\max}$, E_A is the activation energy, and k_B is the Boltzmann constant. In our analysis, the ω_0 is assumed to be temperature independent.[29] The activation energies for different biases can then be deduced from the Arrhenius plot of ω vs $1/T_{\max}$. By the use of Eq. (2.1), the activation energies for different bias voltages can be obtained from the Arrhenius plots, which are displayed in Fig. 4. For each bias, the *G*-*T* spectra were taken at ten measurement frequencies ranging from 1 kHz to 1 MHz. As shown in Fig. 4, the activation

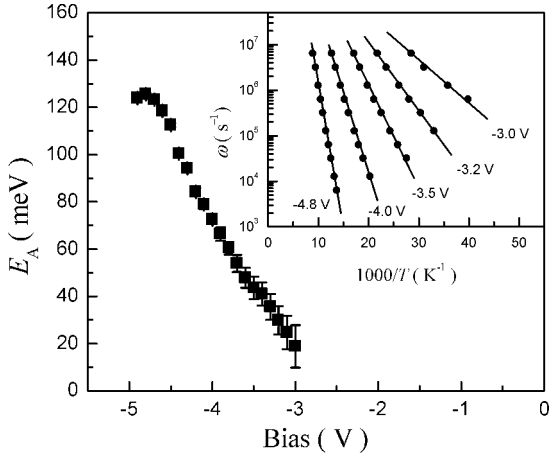

FIG. 4. The deduced activation energies (E_A) as a function of the bias voltages (U). The inset shows the Arrhenius plots for $U=-3.5$ V to $U=-4.8$ V.

energy is $E_A=125$ meV at $U=-4.8$ V, then quasicontinuously decreases to $E_A=18\pm5$ meV as the bias increases up to $U=-3$ V.

III. DISCUSSION

As shown in Fig. 2(a), the *C*-*V* characteristics are quasistatic for $T>100$ K. As a first approximation, the width of the capacitance plateau ΔU can be used to estimate the amount of hole accumulations by $Q\approx C\Delta U$, where C is the average capacitance of the plateau. For $\Delta U\sim1.6$ V and $C\sim350$ pF, we estimate a two-dimensional hole density in the QD layer of $p_{\rm dot}\sim3.5\times10^{11}$ cm^{-2}. For a dot density of $\sim3\times10^{10}$cm^{-2}, determined from the TEM studies, the estimated $p_{\rm dot}$ corresponds to about ~12 holes per dot. However, this value may be reduced somewhat, since the WL is also lightly populated, as can be seen from the weak conductance shoulder [indicated by an arrow in Fig. 2(a)] that appears in the 12-K *G*-*V* trace. The effective hole density of state (DOS) can also be estimated from the accumulated holes and the activation energy dispersion ΔE_A. For a $\Delta E_A\approx107$ meV (from $U=-4.8$ V to $U=-3$ V), the effective hole DOS is given by $\sim3\times10^{12}$/eV cm^2. This value is very close to the value observed in Ge/Si QD system,[30] but is about two orders of magnitude smaller than the two-dimensional hole DOS of an InAs quantum well.[31] This low DOS for the QD's may be caused by the Coulomb-charging effects, which will further split the hole-level spacing during the charging of the holes by the applied bias. Furthermore, the charging effects may push some higher excited hole levels into the WL continuum, and hence reduce the effective hole DOS in the QD's.

We now discuss the bias-dependent activation energy. Since the deduced E_A's only represent *apparent* activation energies, extreme care has to be taken in interpreting these data. To relate these E_A's to the hole-level structure, the actual path whereby holes escape from the dots should be identified first. This requires detailed information on the valence-band bending induced by the hole that accumulated in the

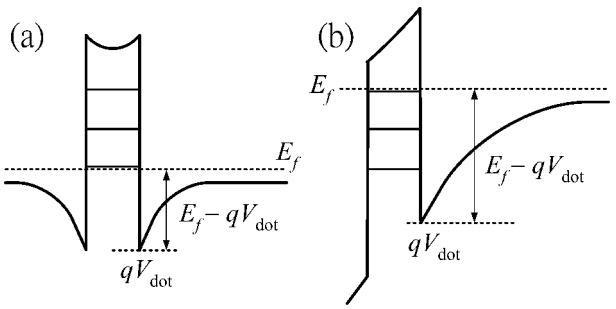

FIG. 5. (a) The valence-band bending near the QD layer when the accumulated holes in the dots are decoupled from the depletion region of the n^+-p junction. (b) The valence-band bending when the holes that have accumulated in the dots have just all been depleted.

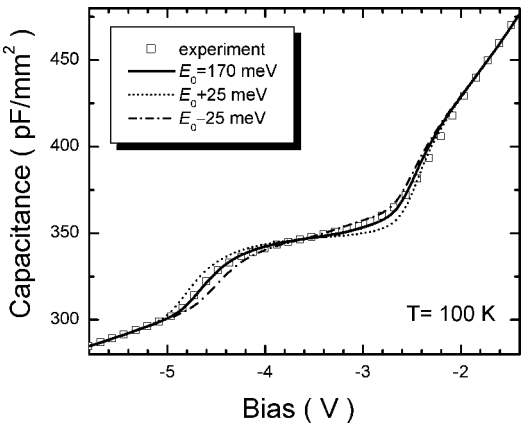

FIG. 6. Self-consistence simulation for the C-V curves measured at $T=100$ K. Except the optimal simulated curve (solid line), two curves with deviation of 25 meV from E_0 are also shown for comparison.

QD layer. However, due to coupling between the depletion width of the n^+-p diode and the density of hole that have accumulated in the dots, the band bending cannot be straightforwardly deduced simply from the depletion approximation. Fortunately, the depletion approximation is still applicable in the following two extreme cases, which can be used to examine the band bending near the QD layer. First, the holes in the QD layer are considered to be decoupled from the depletion region of the n^+-p junction. The band bending in this case can be roughly related to the bias condition, $U\sim -3$ V, which is schematically depicted in Fig. 5(a). From the estimated $p_{\rm dot}$ in the QD layer, the induced valence-band bending (on both sides of the QD layer) can be calculated by a simple depletion approximation, which is estimated to be $qV_{\rm dot}\approx 55\pm 5$ meV. Taking the E_f position into account, the energy difference between E_f and the QD barrier is about $E_f - qV_{\rm dot}\approx 70\pm 5$ meV. Second, consider that all the holes in the QD layer are just depleted, which corresponds to a bias condition of $U\sim -4.8$ V [see Fig. 5(b)]. By using the depletion width determined from the C-V characteristics, an energy difference of $E_f - qV_{\rm dot}\approx 195\pm 15$ meV is estimated.

The quantity of $E_f - qV_{\rm dot}$ represents the barrier height for the hole to be thermally activated into the GaAs valence band. By comparing the activation energy with the estimated barrier heights in both cases discussed above, we found the obtained E_A's to be about 50–70 meV smaller than the corresponding barrier heights. This implies that the hole escape process is not a direct thermal activation process into the GaAs, but instead, a two-step process,[7,8,11] i.e., thermally activated tunneling via an intermediate state situated within the range of 50–70 meV above the GaAs valence-band edge. In this energy range, the most likely intermediate state is the WL. The heavy-hole ground state in the InAs WL can be estimated by the effective mass approximation. For a heavy-hole effective mass of $m_h^* = 0.34 m_0$, the hole ground state of 1.6-ML-thick InAs WL is about $E_{h_{\rm WL}} = 63$ meV above the valence-band edge, which lies just within the energy range of the intermediate state. In other words, the hole escape path is that thermally activated into the WL, and then tunneling out by the assistance of electric field.

For more rigorous calculations, we adapt the quasi-static model proposed by Brounkov *et al.*[9] to simulate the C-V characteristics. This model has been successfully applied to describe the charge distribution and band bending in similar InAs QD systems.[9,32] In this study, the simulation is achieved by self-consistently solving the Poission equation for the whole layer structure. The hole DOS, $D(E)$, of the InAs QD's is described by multiple Gaussian peaks:

$$D(E) = N_{\rm dot} \sum_i \frac{1}{\Gamma\sqrt{\pi/2}} \exp\left[-2\left(\frac{E-E_i}{\Gamma}\right)^2\right], \qquad (3.1)$$

where $N_{\rm dot}$ is the dot density, E_i is the ith hole energy level and Γ is a broadening parameter. Since the QD's may be filled up to ~ 12 holes per dot, it seems impractical to treat the parameters for these hole levels independently. To minimize the number of free parameters, we model the hole level distribution as follows. First, we describe the hole levels by a two-dimensional harmonic oscillator model, with a ground state energy of E_{h0} and a quantization energy of ΔE_h. Second, since the Coulomb-charging effects may be relevant in the hole-level system, we also include a charging energy of E_C in the model calculation. Third, for sake of simplicity, the broadening parameters Γ are assumed to be the same for all levels. Finally, because the WL is considered to be the upper bound for the charging of the hole into the QDs a two-dimensional DOS of the WL at $E_{h_{\rm WL}}$ is also included in this calculation. The $N_{\rm dot}$ is determined independently by TEM measurements, and the doping concentration is deduced from the C-V characteristic itself. The number of fitting parameters are therefore reduced to five, which are E_{h0}, ΔE_h, E_C, $E_{h_{\rm WL}}$ and Γ.

The optimal simulated C-V curve for $T=100$ K is shown in Fig. 6. Despite the crude DOS used here, the simulated result fits the experimental curve fairly well. An optimal simulation shows that the hole ground state is centered at $E_{h0}=170(\pm 5)$ meV, with an inhomogeneous broadening of $\Gamma = 60(\pm 5)$ meV. The determined hole-level splitting and the charging energy are $\Delta E_h = 25(\pm 2)$ meV and $E_C = 13$ (± 2) meV, respectively. The simulation also shows that the

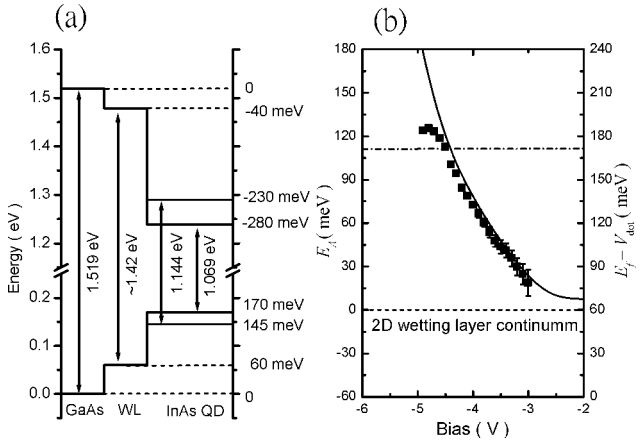

FIG. 7. (a) The energy-level diagram for the investigated InAs/GaAs QD's. (b) A comparison between the deduced activation energies E_A (symbols) and the barrier height $E_f - qV_{\mathrm{dot}}$ (solid line) obtained from the self-consistence simulations. Note that the left and right axes have been offset by 60 meV (see dotted line).

WL is lightly populated, with an energy of $E_{h_{\mathrm{WL}}} = 60$ (± 5) meV above the GaAs valence band.

By combining the determined hole levels and the interband energy acquired from the optical investigations, we can construct the energy-level diagram of the investigated InAs/GaAs QD's, which are summarized in Fig. 7(a). The deduced hole ground state energy, $E_{h0} = 170(\pm 5)$ meV, agrees very well with the theoretical value of 176 meV reported in Ref. 14 for an InAs pyramid of similar ground-state emission energy (1.098 eV), calculated by an eight-band $\mathbf{k}\cdot\mathbf{p}$ model. This value is also comparable with the value of 193 meV reported in Ref. 16, for a lens-shaped dot, calculated using an empirical pseudopotential model. Combining the E_{h0} with the PL results, the ground-state electron localization energy is estimated to be $E_{e0} = 280(\pm 10)$ meV. This value is in excellent agreement with that reported by Chu *et al.*[13] using midinfrared photocurrent spectroscopy on InAs QD's with similar ground-state PL emissions (1.08 eV). This means that the localization energy of the hole is relatively weaker than that of the electron in the investigated InAs/GaAs QD's. For hole-level splitting, the determined $\Delta E_h = 25 \pm 2$ meV is comparable to the value (~ 30 meV) determined by the midinfrared unipolar emission spectra.[33] By combining the hole-level splitting ΔE_h with the interband energy splitting (75 meV) determined from the PL spectra, the electron-level splitting is found to $\Delta E_e \approx 50$ meV. This agrees very well with those determined from capacitance[34] and far-infrared[35] spectroscopies. However, we note that the charging energy $E_C = 13(\pm 2)$ meV determined from our simulations is somewhat smaller than the theoretically predicted values (20–30 meV) for similar sized dots. This may be due the fact that the E_C is also occupation dependent. As has been shown in Ref. 36, for a two-dimensional harmonic oscillator, the direct Coulomb interaction will get smaller for the higher hole excited states. Thus, the constant E_C used in our model calculation may present an average value. Moreover, in our calculations the charge distribution is reduced to an effective one-dimensional electrostatic problem. A more extended investigation is needed to deal with the electrostatic problems using a three-dimensional approach.

After the numerical simulations, we can now compare the deduced E_A's with the barrier height $E_f - qV_{\mathrm{dot}}$ for the full bias range, which are shown in Fig. 7(b). For comparison purposes, these E_A values have been offset by a constant energy of $E_{h_{\mathrm{WL}}} = 60$ meV. In this figure, the simulated $E_f - qV_{\mathrm{dot}}$ agrees very well with the obtained E_A's, when the $E_{h_{\mathrm{WL}}}$ is included as an intermediate state.

In Ref. 11, we have determined that the electron emission process is dominated by thermally activated tunneling via the available excited states. This is similar to the assignment reported by Kapteyn *et al.*[7,8] using DLTS measurements. The hole emission process found in the current study is also a thermally activated tunneling process, but the intermediate state is the hole's WL state instead of the excited states of the dots. However, the work reported by Kapteyn *et al.*[8] has suggested that hole emission is a direct activation process. In fact, a large variety of emission processes can be found in different published works, even the same experimental techniques have used. For example, a direct activation process for both electron and hole escape has also been suggested by Wang *et al.*[15] after their DLTS studies, while the DLTS results reported by Ibáñez *et al.*[18] showed the tunneling escape process to be important for both the electron and the hole.

To resolve these apparent discrepancies, we intend to construct in the following a general picture of the carrier emission processes. In general, the carrier emission processes are not only determined by the inherent properties of the QD's, but also by the environmental conditions. The most important inherent property is the carrier localization energy, since they directly determine the thermionic emission rates from a given QD level to the band edge. Some other inherent properties in the QD's are also relevant, for example, the energy-level splitting and the carrier effective mass. The most important factor for the environmental conditions is the electric field, which is either internally exhibited in the designed structures or externally applied during the experiments. Some other effects may be also relevant, such as intentional modification of the barrier height using $\mathrm{Al}_x\mathrm{Ga}_{1-x}\mathrm{As}$ (Ref. 4) or $\mathrm{In}_x\mathrm{Ga}_{1-x}\mathrm{As}$ (Ref. 39) instead of GaAs. In this work, we conclude that the hole localization is weaker than the electron localization. This means that the electron escape rate will be slower than that of the hole, if only thermionic emissions into the barrier are considered. However, this situation may change when the electric field is presented. As shown in Fig. 8, the electric field can cause the higher excited QD states to become quasistationary. Thus, thermally activated tunneling via these quasistationary states becomes possible. The total escape rate $(1/\tau_{\mathrm{tot}})$ for such thermally activated tunneling can then be determined by the product of the thermionic emission rate $(1/\tau_{\mathrm{th}})$ and the tunneling rate $(1/\tau_{\mathrm{tun}})$.

As schematically depicted in Fig. 8, both the $1/\tau_{\mathrm{th}}$ and the $1/\tau_{\mathrm{tun}}$ depend exponentially on E, but have opposing tendencies. This means that the total escape rate will reach a maximum at a certain optimal energy E_{opt}, depending on the electric field and the effective mass. This optimal energy plays a decisive role in both the electron and the hole escape

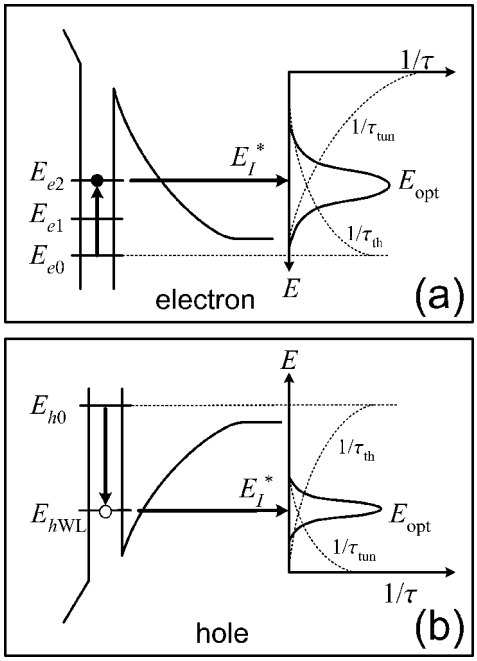

FIG. 8. The thermally activated tunneling processes for electrons (a) and holes (b) escaping from the QD's via optimal prospective intermediate states.

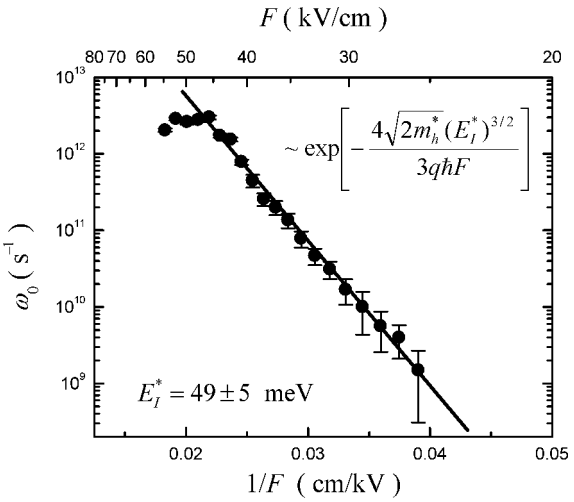

FIG. 9. The ω_0 as a function of the inverse electric field $1/F$. The ω_0's are obtained from the Arrhenius plot at different bias voltages, while the electric fields F are deduced from the self-consistent simulations.

processes. For the electron escape process, shown in Fig. 8(a), due its smaller effective mass, the $E_{\rm opt}$ can be deeper. The electron can find an available excited state near the $E_{\rm opt}$ as an optimal intermediate state (E_I^*) for the subsequent tunneling process. In this case, the escape of ground-state electrons tends to be mediated by the first or the second excited states, as reported in Ref. 8 and Ref. 11, depending on the field strength, the interlevel splitting of the QD's, and the temperature. For the hole escape process shown in Fig. 8(b), since the effective mass of the hole is about 5–10 times larger than that of the electron, the optimal energy $E_{\rm opt}$ will be pushed toward the valence-band edge, and hence the shallower WL state becomes the favored intermediate state. For a lower electric field, the hole tunneling will be further suppressed, and hence the holes can even be directly activated into the valence band. This is the situation observed in Ref. 8.

A simple way to further analyze this thermally activated tunneling is to approximate the $V(z)$ by using a linear potential, i.e., $V(z)=qFz$, where q is the electrical charge and F is the electric field. Thus, the tunneling rate can then be approximated by an effective one-dimensional confining potential[37,38] of width L_z. The total escape rate is then given by

$$\frac{1}{\tau_{\rm tot}} \sim \frac{\hbar\pi}{2m^* L_z^2} \exp\left(-\frac{4\sqrt{2m^*}(E_I^*)^{3/2}}{3q\hbar F}\right) \times \exp\left(-\frac{E_h - E_I^*}{k_B T}\right), \tag{3.2}$$

where E_h is a given hole level and L_z can be taken as the dot height (3.5 ± 5 nm). By comparing Eq. (2.1) and Eq. (3.2), one finds that the tunnelling rate is involved in the pre-exponential factor, i.e., $\omega_0 \propto 1/\tau_{\rm tun}$. Therefore, the ω_0 obtained from the Arrhenius plots (the inset to Fig. 9) can be further used to analyze the hole tunneling barrier height. According to the self-consistence simulations, the electric field crossing the QD layer increases from $F\approx25$ kV/cm at $U=-3$ V to $F\approx52$ kV/cm at $U=-4.8$ V. Therefore, plotting the obtained ω_0 as a function of $1/F$ can be used to determine the tunneling barrier height of the intermediate state, as shown in Fig. 9. From the apparent slope, and assuming a hole effective mass of $m^*=0.34m_0$, the tunneling barrier height is estimated to be $49(\pm5)$ meV, which is comparable to the hole energy level of the WL.

According to Eq. (3.2), it is now possible to qualitatively compare the electron and hole emission rates, which may enable us to get a closer look at the underlying mechanism of exciton dissociation from the dots. This subject has been investigated by different groups using temperature-dependent photocurrent (PC) spectroscopy.[12,39,40] Interestingly, the deduced thermal activation energies are quite small, typically 2–3 times smaller than the corresponding exciton localization energies.[12,39,40] Such a small activation energy has been attributed to the thermally activated tunneling of less-confined holes in the dots.[39] However, Brounkov *et al.*[12] argue that the PC is mainly controlled by the thermal escape of electrons out of the dots. This discrepancy may be resolved by comparing the optimal escape rates of electrons and holes using Eq. (3.2). In Fig. 10(a), we first compare the emission rates for more deeply confined electrons ($E_{e0}=280$ meV) and weakly confined holes ($E_{h0}=170$ meV) under different electric fields at a typical temperature of $T=100$ K. We set the electron's and hole's effective masses to be $m_e^*=0.04m_0$ and $m_h^*=0.34m_0$, respectively. For $F=50$ kV/cm, the optimal emission rate for the electron is almost ~4 orders of magnitude slower than the hole's. Even when the electric field is increased up to $F=80$ kV/cm the thermally activated tunneling of the hole is still more relevant, due to its weaker localization energy. However, this situation will be inverted when the holes become more

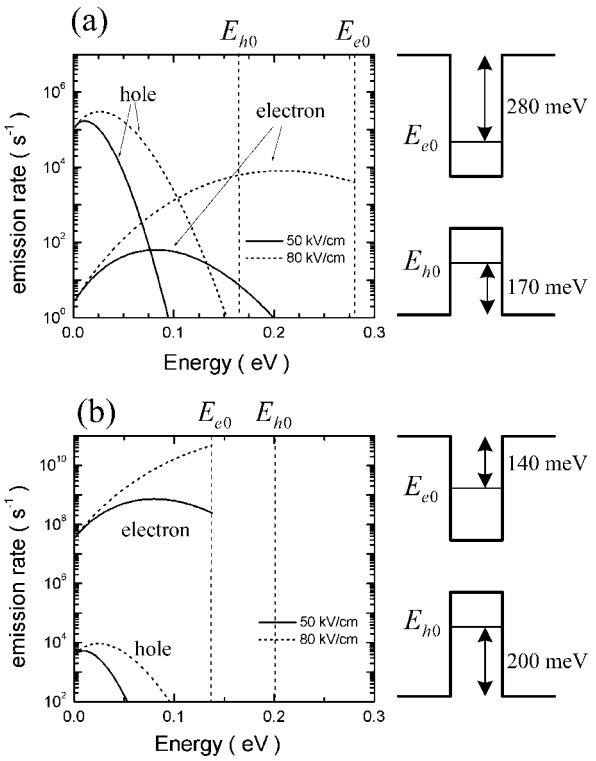

FIG. 10. The electron and hole escape rates for different electric fields and localization energies: (a) $E_{e0}=280$ meV and $E_{h0}=170$ meV; (b) $E_{e0}=140$ meV and $E_{h0}=200$ meV.

deeply confined. This behavior is displayed in Fig. 10(b), where the electron and hole localization energies are set to be $E_{e0}=140$ meV and $E_{h0}=200$ meV, i.e., the values reported in Ref. 12. In this case, the electron escape process becomes considerably faster that of the hole, which may explain why the temperature dependence of PC spectra, observed in Ref. 12, was controlled by the thermal escape of the electrons. From the above comparative analysis, it can be concluded that both the localization energy and the electric field are important for the carrier emission processes. In other words, whenever one intends to identify which carrier type would be more relevant during the QD exciton dissociations, both the localization energy of the dots and the electric-field conditions should be carefully examined.

IV. CONCLUSIONS

In summary, the hole emission processes in InAs/GaAs QD's are investigated by capacitance and admittance spectroscopy. From the conductance mapping spectroscopy, the hole-level distribution is found to be quasicontinuous, indicating that the hole-level splitting in the QD's is smaller than the inhomogeneous broadening. The admittance spectroscopy shows that the apparent activation energies are in the range of 18–125 meV, depending on the applied reversed bias. The main path for the holes to escape from the dots is a two-step process, i.e., thermal activation to an intermediate state and then subsequent tunneling out assisted by the electric field. The intermediate state for the hole is found to be the wetting layer, rather than the available excited states that have been found in electron system. A generalized model of thermally activated tunneling is constructed to explain the differences between the electron and hole escape processes. It is found that the emission rates for both carrier types depend sensitively on the localization energies and the electric field crossing the dots. This means that both the localization energies of the dots and the applied electric field will determine which carrier type would be more relevant during the QD exciton dissociations.

ACKNOWLEDGMENTS

This work was supported in part by the National Science Council of the Republic of China under Grant No. NSC89-2112-M-008-063.

*Electronic address: tmhsu@phy.ncu.edu.tw

[1] Y. Arakawa and H. Sakaki, Appl. Phys. Lett. **40**, 939 (1982).
[2] L. Chu, A. Zrenner, M. Bichler, and G. Abstreiter, Appl. Phys. Lett. **79**, 2249 (2001).
[3] Zhonghui Chen, Eui-Tae Kim, and Anupam Madhukar, Appl. Phys. Lett. **80**, 2490 (2002).
[4] T. Lundstrom, W. Schoenfeld, H. Lee, and P.M. Petroff, Science **286**, 2312 (1999).
[5] For a recent review, see for example: D. Bimberg, M. Grundmann, and N. N. Ledentsov, *Quantum Dot Heterostructures* (Wiley, Chichester, 1999).
[6] G. Medeiros-Ribeiro, D. Leonard, and P.M. Petroff, Appl. Phys. Lett. **66**, 1767 (1995).
[7] C.M.A. Kapteyn, F. Heinrichsdorff, O. Stier, R. Heitz, M. Grundmann, N.D. Zakharov, D. Bimberg, and P. Werner, Phys. Rev. B **60**, 14 265 (1999).
[8] C.M.A. Kapteyn, M. Lion, R. Heitz, D. Bimberg, C. Miesner, T. Asperger, K. Brunner, and G. Abstreiter, Appl. Phys. Lett. **77**, 4169 (2000).
[9] P.N. Brounkov, A. Polimeni, S.T. Stoddart, M. Henini, L. Eaves, P.C. Main, A.R. Kovsh, Yu.G. Musikhin, and S.G. Konnikov, Appl. Phys. Lett. **73**, 1092 (1998).
[10] P.N. Brunkov, A.R. Kovsh, V.M. Ustinov, Y.G. Musikhin, N.N. Ledentsov, S.G. Konnikov, A. Polimeni, A. Patanè, P.C. Main, L. Eaves, and C.M.A. Kapteyn, J. Electron. Mater. **28**, 486 (1999).
[11] W.-H. Chang, W.Y. Chen, M.C. Cheng, C.Y. Lai, T.M. Hsu, N.-T. Yeh, and J.-I. Chyi, Phys. Rev. B **64**, 125315 (2001).
[12] P.N. Brunkov, A. Patanè, A. Levin, L. Eaves, P.C. Main, Yu.G. Musikhin, B.V. Volovik, A.E. Zhukov, V.M. Ustinov, and S.G. Konnikov, Phys. Rev. B **65**, 085326 (2002).
[13] L. Chu, A. Zrenner, G. Böhm, and G. Abstreiter, Appl. Phys. Lett. **76**, 1944 (2000).
[14] O. Stier, M. Grundmann, and D. Bimberg, Phys. Rev. B **59**, 5688 (1999).
[15] L.-W. Wang, J. Kim, and A. Zunger, Phys. Rev. B **59**, 5678 (1999).
[16] A.J. Williamson, L.-W. Wang, and A. Zunger, Phys. Rev. B **62**, 12 963 (2000).
[17] R.J. Luyken, A. Lorke, A.O. Govorov, J.P. Kotthaus, G.

Medeiros-Ribeiro, and P.M. Petroff, Appl. Phys. Lett. **74**, 2486 (1999).

[18] J. Ibáñez, R. Leon, D.T. Vu, S. Chaparro, S.R. Johnson, C. Navarro, and Y.H. Zhang, Appl. Phys. Lett. **79**, 2013 (2001).

[19] H.L. Wang, F.H. Yang, S.L. Feng, H.J. Zhu, D. Ning, H. Wang, and X.D. Wang, Phys. Rev. B **61**, 5530 (2000).

[20] D.V. Lang, J. Appl. Phys. **45**, 3023 (1974).

[21] D.V. Lang, M.B. Panish, F. Capasso, J. Allam, R.A. Hamm, A.M. Sergent, and W.T. Tsang, Appl. Phys. Lett. **50**, 736 (1987).

[22] X. Letartre, D. Stievenard, M. Lannoo, and D. Lippens, J. Appl. Phys. **68**, 116 (1990).

[23] B.L. Stein, E.T. Yu, E.T. Croke, A.T. Hunter, T. Laursen, A.E. Bair, J.W. Mayer, and C.C. Ahn, Appl. Phys. Lett. **70**, 3413 (1997).

[24] R. Heitz, T.R. Ramachandran, A. Kalburge, Q. Xie, I. Mukhametzhanov, P. Chen, and A. Madhukar, Phys. Rev. Lett. **78**, 4071 (1997).

[25] R. Heitz, M. Veit, N.N. Ledentsov, A. Hoffmann, D. Bimberg, V.M. Ustinov, P.S. Kop'ev, and Zh.I. Alferov, Phys. Rev. B **56**, 10 435 (1997).

[26] The estimation of WL thickness ($\sim$1.6 ML) is based on effective-mass approximation of pure InAs quantum well excluding the effects of QD's thereon. However, this effective thickness may be reduced somewhat (1.3–1.4 ML) if the WL is considered as an $In_xGa_{1-x}As$ quantum well, which would be more reasonable as compared with the structural and optical investigations reported in Ref. 24 and Ref. 25.

[27] T.M. Hsu, W.-H. Chang, K.F. Tsai, J.-I. Chyi, N.T. Yeh, and T.E. Nee, Phys. Rev. B **60**, R2189 (1999).

[28] W.-H. Chang, T.M. Hsu, N.T. Yeh, and J.-I. Chyi, Phys. Rev. B **62**, 13 040 (2000).

[29] The factor ω_0 may be also temperature-dependent. For a system containing deep traps, a T^2 dependence is commonly included. A T dependence has also been used in quantum-well and superlattice systems. But for a QD system, it is not *a priori* clear how the preexponential factor depends on temperature. This requires detailed knowledge of the temperature dependence of the hole being captured by the QD's. Without having detailed information on the hole capture mechanism, the ω_0 is assumed to be temperature-independent in our analysis.

[30] C. Miesner, T. Asperger, K. Brunner, and G. Abstreiter, Appl. Phys. Lett. **77**, 2704 (2000).

[31] For a heavy-hole effective mass of $m_h^*=0.34m_0$ in an InAs quantum well, the effective density of state is $m_h^*/\pi\hbar^2=1.4\times10^14\ \mathrm{eV}^{-1}\,\mathrm{cm}^{-2}$.

[32] R. Wetzler, A. Wacker, E. Scholl, C.M.A. Kapteyn, R. Heitz, and D. Bimberg, Appl. Phys. Lett. **77**, 1671 (2000).

[33] S. Sauvage, P. Boucaud, T. Brunhes, A. Lemaître, and J.-M. Gérard, Phys. Rev. B **60**, 15 589 (1999).

[34] K.H. Schmidt, G. Medeiros-Ribeiro, M. Oestreich, P.M. Petroff, and G.H. Döhler, Phys. Rev. B **54**, 11 346 (1996).

[35] M. Fricke, A. Lorke, J.P. Kotthaus, G. Medeiros-Ribeiro, and P.M. Petroff, Europhys. Lett. **36**, 197 (1996).

[36] R.J. Warburton, B.T. Miller, C.S. Dürr, C. Bödefeld, K. Karrai, J.P. Kotthaus, G. Medeiros-Ribeiro, P.M. Petroff and S. Huant, Phys. Rev. B **58**, 16 221 (1998).

[37] David M.-T. Kuo and Y.C. Chang, Phys. Rev. B **61**, 11 051 (2000).

[38] P.W. Fry, J.J. Finley, L.R. Wilson, A. Lemaitre, D.J. Mowbray, M.S. Skolnick, M. Hopkinson, G. Hill, and J.C. Clark, Appl. Phys. Lett. **77**, 4344 (2000).

[39] W.-H. Chang, T.M. Hsu, C.C. Huang, S.L. Hsu, C.Y. Lai, N.T. Yeh, T.E. Nee, and J.-I. Chyi, Phys. Rev. B **62**, 6959 (2000).

[40] P.W. Fry, I.E. Itskevich, S.R. Parnell, J.J. Finley, L.R. Wilson, K.L. Schumacher, D.J. Mowbray, M.S. Skolnick, M. Al-Khafaji, A.G. Cullis, M. Hopkinson, J.C. Clark, and G. Hill, Phys. Rev. B **62**, 16 784 (2000).